Fingerprint Classification Using Orientation Field Flow Curves

Sarat C. Dass
Michigan State University
sdass@msu.edu

Anil K. Jain
Michigan State University
jain@msu.edu

Abstract

Manual fingerprint classification proceeds by carefully inspecting the geometric characteristics of major ridge curves in a fingerprint image. We propose an automatic approach of identifying the geometric characteristics of ridges based on curves generated by the orientation field called orientation field flow curves (OFFCs). The geometric characteristics of OFFCs are analyzed by studying the isometric maps of tangent planes as a point traverses along the curve from one end to the other. The path traced by the isometric map consists of several important features such as sign change points and locations as well as values of local extremas, that uniquely identify the inherent geometric characteristics of each OFFC. Moreover, these features are invariant under changes of location, rotation and scaling of the fingerprint. We have applied our procedure on the NIST4 database consisting of 4,000 fingerprint images without any training. Classification into four major fingerprint classes (arch, left-loop, right-loop and whorl) with no reject options yields an accuracy of 94.4.%

1. Introduction

Fingerprint classification is a coarse level partitioning of a large fingerprint database, where the class of the input fingerprint is first determined and subsequently, a search is conducted within the set of fingerprints belonging to the same class as the input fingerprint. In this work, we classify fingerprint images into 4 major classes in the Henry classification system [5]: arch, left-loop, right-loop and whorl. The arch class can be further divided into two subclasses consisting of the plain arch and tented arch. These 5 classes of fingerprints in the Henry classification system are shown in Figure 1. While the Henry classification system has many classes, only 4, 5 or 7 classes have been used in an automatic classification procedure. The reason for using only a small number of classes is because the task of determining a fingerprint class can be difficult. Important fingerprint features that aid classification exhibit large variations, thus, making the task of representing these features in an automatic system challenging. Sometimes, even human experts label the same fingerprint as being of different classes; for example, 700 fingerprints out of the 4,000 fingerprints in the NIST4 database [15] have two different class labels associated with them.

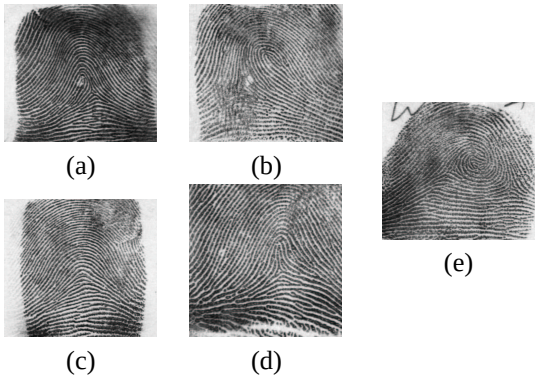

Figure 1. Five classes of fingerprints in the Henry system: (a) left-loop, (b) right-loop, (c) arch, (d) tented arch, and (e) whorl. Images are from the NIST4 database [15].

2. Previous Work on Fingerprint Classification

A number of approaches have been developed for automatic fingerprint classification. These approaches can be grouped into five main categories: (i) approaches based on singular points [6, 8], (ii) structure-based [1, 2, 3], (iii) frequency-based [7], (iv) syntactic or grammar-based [11], and (v) approaches based on mathematical models [10]. Hybrid methods combine at least two approaches in (i-v) to arrive at a fingerprint classification algorithm (see, for example, [2, 3]). Some of the hybrid methods have not been tested on large databases; for example, Chong et al [3] used 89 fingerprint images. Table 1 compares the classification accuracies obtained by several fingerprint classification methods reported in the literature.

Table 1. A comparison of classification accuracies (in %) of several fingerprint classification methods in the literature. Reject rates are also given in percentages.

Method	No.	4 class	5 class	Reject Rate
Cappelli et al [1]	$1,204$	-	87.1^a	0.0
Chang & Fan [2]	$2,000$	-	94.8	5.1
Chong et al [3]	89	-	96.6^b	0.0
Hong & Jain [6]	$4,000$	92.3	87.5	0.0
Jain et al [7]	$4,000$	94.8	90.0	0.0
Karu & Jain [8]	$4,000$	91.4	85.4	0.0
Minut & Jain [10]	$4,000$	91.2	-	0.0
Wilson et al [16]	$4,000$	-	94.0^c	10.0
Dass & Jain	$4,000$	94.4	-	0.0

[a] using the natural distribution of fingerprints
[b] based on the 5 classes - double loop, whorl, left-loop, right-loop and arch
[c] using the natural distribution of fingerprints; equal distribution of each class yields accuracies of $84 - 88\%$.

The most natural topology for analyzing fingerprint images is the topology of curves created by the ridge and valley structures. This necessitates the use of methods from differential geometry for the analysis of properties of the curves, or curve features. The approach presented in this paper is a combination of the structure-, syntactic- and mathematical-based approaches. For a given fingerprint image to be classified, the algorithm first extracts an orientation field for the fingerprint image. Next, orientation field flow curves (OFFCs) are generated based on the estimated orientation field. There are two advantages of using OFFCs for fingerprint classification: (i) unlike ridge curve extraction, breaks and discontinuities in the OFCCs are avoided, and (ii) the OFFCs are free from small scale ridge oscillations. Each flow curve is then labelled as either loop (left or right), whorl or arch depending on its intrinsic geometric structure. Rigid mathematical models as in [10] are not adequate for representing all aspects of variability of the OFFCs. We develop robust procedures based on differential geometry for labelling the OFFCs. The geometric characteristics of OFFCs are analyzed by studying the changes occurring in the tangent space as a point traverses along a OFFC from one end to the other. The tangent space at each point along an OFFC is isometrically mapped to a reference tangent space. The path traced by the isometric map consists of several important features such as sign change points, locations as well as values of local extremas, that uniquely identify the inherent geometric characteristics of each OFFC. Moreover, since the methodology is derived from differential geometry, these features are invariant under changes of location, rotation and scale. Based on these features, we are able to label the OFFCs into four classes, namely, left- and right-loops, whorl and arch. Subsequently, the labels the OFFCs are processed based on syntactic rules to arrive at a fingerprint class. We have applied our procedure on the NIST4 database consisting of 2,000 fingerprint images. Classification into 4 classes of the Henry system results in an accuracy of 94.4% with no reject options. We note that our classification accuracy is comparable to the ones reported in the literature (see Table 1).

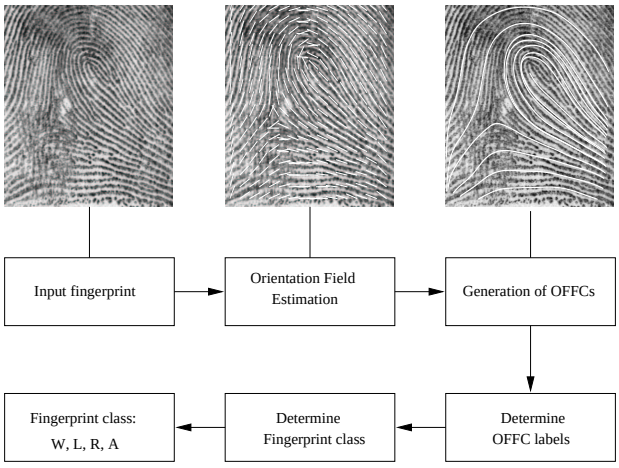

Figure 2. Steps involved in determining the class of a fingerprint.

3. General Methodology

3.1. Generating Orientation Field Flow Curves

Our approach to fingerprint classification involves four major steps: (i) the extraction of the orientation field for the given fingerprint image, (ii) generation of orientation field flow curves (OFFCs), (iii) labelling of each OFFC into the four classes: left- and right-loops, whorl and arch, and (iv) an overall classification of the fingerprint image into one of the four classes based on syntactic rules. Figure 2 shows the steps involved in classifying a fingerprint image.

Consider a site s in a fingerprint image $\mathcal{I}$ with r rows and c columns. The orientation field of $\mathcal{I}$ gives the direction of the ridge flow in a local neighborhood around s for all $s \in \mathcal{I}$. The value of the orientation at site s, o_s, is a vector $(\cos\theta_s, \sin\theta_s)^T$ where θ_s is the angle of the flow with respect to the horizontal axis. Opposite flow directions are equivalent, and therefore, θ_s can only be determined uniquely in $(-\pi/2, \pi/2)$. There are many algorithms in the literature that find orientations based on the gray intensities of a given image. However, the orientation field estimation

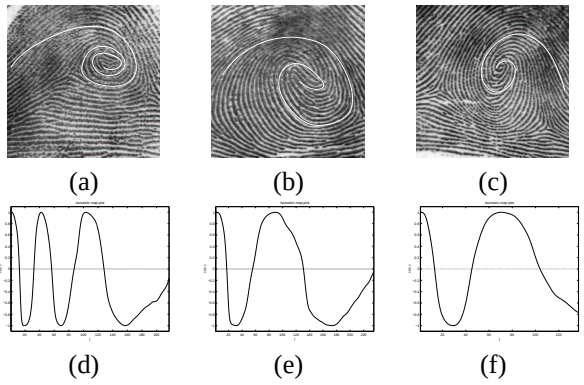

Figure 3. Variations in whorl curves: OFFCs (white curves) labelled as whorls in panels (a-c) with corresponding graphs of cos γ_j versus j in panels (d-f)

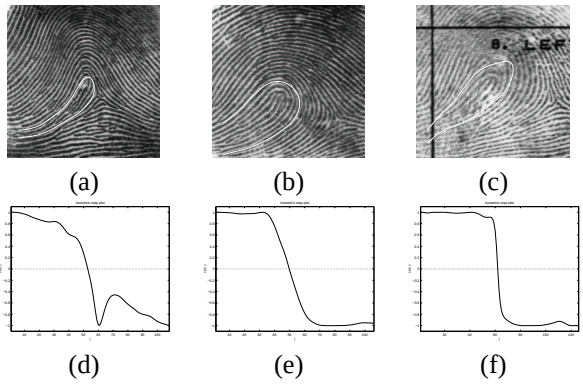

Figure 4. Variations in left-loop curves: OFFCs (white curves) labelled as whorls in panels (a-c) with corresponding graphs of cos γ_j versus j in panels (d-f)

algorithm reported in [4] was specially designed for fingerprint images taking into account the smoothness of the orientations at sites in the image that are close to each other. Hence, a more robust orientation field estimate results (see [4] for further details). The orientation field estimate is obtained for sites $s = (x, y)$ in $\mathcal{I}$ where x and y are integers such that $1 \leq x \leq r$ and $1 \leq y \leq c$. In order to obtain the value of the ridge orientation at any site $s = (x, y)$ in $\mathcal{I}$, we adopt an interpolation scheme. Let m and n be integers such that $m = [x]$ and $n = [y]$, where $[g]$ stands for the greatest integer less than or equal to g. The orientation vector at site $s = (x, y)$ is given by $o_s = (\cos\theta_s, \sin\theta_s)^T$ where

$$\theta_s = \frac{1}{2}\tan^{-1}\frac{\sum_{(i,j)\in\{0,1\}^2} u_i\, v_j \sin 2\theta_{(m+i,n+j)}}{\sum_{(i,j)\in\{0,1\}^2} u_i\, v_j \cos 2\theta_{(m+i,n+j)}}, \quad (1)$$

with $u_0 = m + 1 - x$, $u_1 = 1 - u_0$, $v_0 = n + 1 - y$, and $v_1 = 1 - v_0$. The interpolation scheme in (1) is a weighted average of orientation field values at the integer sites (m, n), $(m, n + 1)$, $(m + 1, n)$ and $(m + 1, n + 1)$. The weights are given by $u_i v_j$ with (i, j) taking values in $\{0, 1\}^2$. The interpolation scheme in (1) yields a value of orientation for all sites $s \in \mathcal{I}$ while retaining the original values at the integer sites.

An OFFC with a starting point $s_0 \in \mathcal{I}$ can be defined iteratively as

$$s_j = s_{j-1} + d_j \cdot l_j \cdot o_{s_{j-1}} \quad (2)$$

for $j = 1, 2, \ldots, n$; d_j, with values in $\{-1, +1\}$, is the flow direction from s_{j-1} to s_j, l_j is the length of the line segment from s_{j-1} to s_j, and $o_{s_{j-1}}$ is the orientation vector at site s_{j-1}. The point s_n denotes the termination point of the OFFC curve, which is achieved when either (i) the boundaries of the image is reached, or (ii) when n exceeds a prespecified constant N_0. The lengths l_j specify the sampling interval of the OFFC. In this paper, we select a common l_j for all the OFFCs, that is, $l_j = l$, say. Each point s_0 generates two segments of an OFFC which are obtained by fixing d_1 first at $+1$, and then at -1, so that the points s_j in (2) trace opposite directions. The starting points s_0 are selected in the following way: Let r_{start}, r_{end}, c_{start} and c_{end} determine the top, bottom, left and right boundaries of the fingerprint pattern area, and w denote the sampling width. The points s_0 are selected such that

$$s_0 = (r_{start} + k\, w\, , c_{start} + l\, w), \quad (3)$$

with either (i) $k = 1, 2, \ldots, [\frac{r_{end}-r_{start}}{w}]$ and $l = [\frac{c_{end}-c_{start}}{2w}]$ or, (ii) $k = [\frac{r_{end}-r_{start}}{2w}]$ and $l = 1, 2, \ldots, [\frac{c_{end}-c_{start}}{w}]$. In other words, the starting points are sampled along the horizontal and vertical lines that pass through the midsection of the fingerprint pattern area. Figure 2 shows how the OFFCs are generated given a fingerprint image. We proceed with the labelling of each OFFC curve using methods developed from differential geometry [14] in the next section.

3.2. Tangent space isometric maps of OFFCs

Our goal in this section is to label each OFFC into one of the four classes based on their global geometric shapes: left- and right-loops, arch and whorl (see the left panels of Figures 3, 4, 5 and 6 for examples of each class). Obtaining explicit mathematical models for the global geometric characteristics of OFFCs will often be too rigid to adequately represent all possible variations of these curves. Therefore, we adopt a non-model based approach here. We discuss several robust features of the OFFCs that allow us to infer

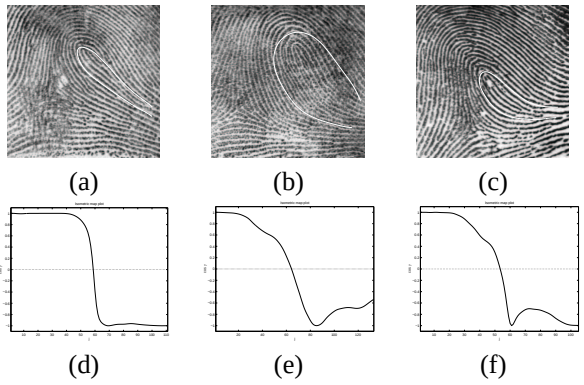

Figure 5. Variations in right-loop curves: OFFCs (white curves) labelled as whorls in panels (a-c) with corresponding graphs of cos γ_j versus j in panels (d-f)

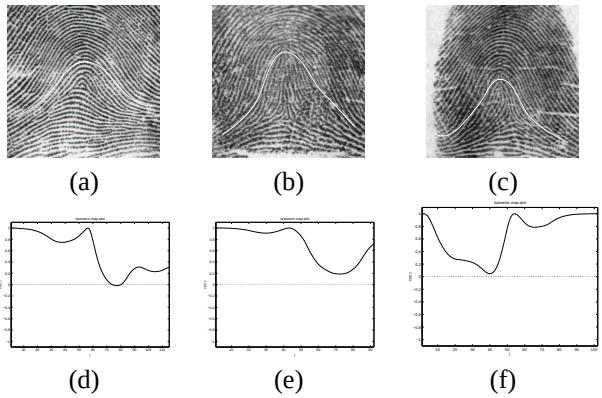

Figure 6. Variations in arch curves: (OFFCs (white curves) labelled as whorls in panels (a-c) with corresponding graphs of cos γ_j versus j in panels (d-f)

the underlying class based on methods of differential geometry.

Let $\alpha(t) \equiv (\alpha_1(x(t), y(t)), \alpha_2(x(t), y(t)))^T$ with $t \in [t_0, t_1]$ denote a curve in the R^2 plane passing through the point (x_0, y_0). The tangent vector at (x_0, y_0) is $(\alpha_1^{'}(x_0, y_0), \alpha_2^{'}(x_0, y_0))^T$, where the derivative is taken with respect to t. We define $V_{(x_0,y_0)}$ to be the translation of $(\alpha_1^{'}(x_0, y_0), \alpha_2^{'}(x_0, y_0))^T$ so that the starting point of $V_{(x_0,y_0)}$ is at the origin $(0, 0)$. The tangent plane, $T_{(x_0,y_0)}$, at point (x_0, y_0) for the curve α is a one-dimensional plane generated by the tangent vector $V_{(x_0,y_0)}$, that is,

$$T_{(x_0,y_0)} = \{u \cdot V_{(x_0,y_0)} \, : \, u \in R\}. \tag{4}$$

In other words, $T_{(x_0,y_0)}$ is the set of all tangent vectors at the point (x_0, y_0) translated to the origin.

Any mapping of points in the plane, $F : R^2 \rightarrow R^2$ has a tangent map F_* that carries each tangent vector v at point p to a tangent vector $F_*(v)$ at point $F(p)$. The map F is said to be an isometry if it preserves distances, that is,

$$d(p, q) = d(F(p), F(q)), \tag{5}$$

where d is the Euclidean distance in R^2. In the case of an isometric map, the tangent map, F_*, is very simple to describe: each tangent vector v at p is "rotated" in exactly the same way by F_*, and translated to the point $F(p)$. In other words, the tangent map F_*, modulo translations, can be uniquely described by a rotation angle γ.

For a given OFFC, we compute the isometric maps as follows: Let one end point of the curve be denoted by p_0 and the other by p_N. Our analysis is not affected by which end is selected as p_0. Define the chord vector $V_1 \equiv \frac{1}{\delta}(x_1 - x_0 \, , \, y_1 - y_0)^T$, where $p_0 \equiv (x_0, y_0)$, and $p_1 \equiv (x_1, y_1)$ is a point on the curve at a distance δ from p_0. The plane spanned by V_1 is denoted by T_1, and the unit vector by $e_1 \equiv V_j/||V_j||$. Subsequent chord vectors, V_j, are obtained as $V_j \equiv \frac{1}{\delta}(x_j - x_{j-1} \, , \, y_j - y_{j-1})^T$, where $p_j \equiv (x_j, y_j)$ are points on the curve at a distance δ apart for $j = 2, \ldots, N$, with the spanned plane denoted by T_j, and the unit vector by $e_j \equiv V_j/||V_j||$. Note that T_j coincides with the tangent plane of some points ξ_j on the OFFC which lies between p_{j-1} and p_j, for $j = 1, 2, \ldots, N$. With T_1 as the reference plane, we obtain the isometric maps F_*s in terms of the rotation angles γ_j that is needed to rotate the plane T_1 to match T_j, with $\gamma_1 \equiv 0$. The feature we consider is the cosine of γ_j which can be obtained as

$$\cos \gamma_j = e_1 \bullet e_j \tag{6}$$

for $j = 1, 2, \ldots, N$, where $\bullet$ is the Euclidean inner product on R^2. The right panels of Figures 3, 4, 5 and 6 show the graphs of $\cos \gamma_j$ versus j as the point on an OFFC traverses from p_0 to p_N for the classes whorl, right-loop and arch, respectively.

3.3. Salient Features Of Isometric Maps

Figures 3-6 give the isometric map plots obtained for the different classes of OFFCs: left-loop, right-loop, whorl and arch. Salient features of the graphs are (i) the number and locations of sign-change points, and (ii) the number and locations of local maximums and minimums. These features are robust with respect to variations within each curve class.

Figures 3 (b), (d) and (f) give the graphs of the isometric maps for several different OFFCs of type whorl (indicated by a white curve in the corresponding left panels). The salient features (comparing Figures 3 (b), (d) and (f)) of the isometric map plots include: (i) several (more than

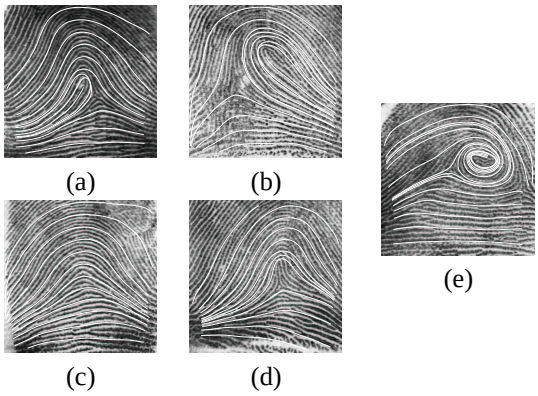

Figure 7. OFFCs for the five different classes (a) left-loop, (b) right-loop, (c) arch, (d) tented arch, and (e) whorl. All these fingerprints have been correctly classified.

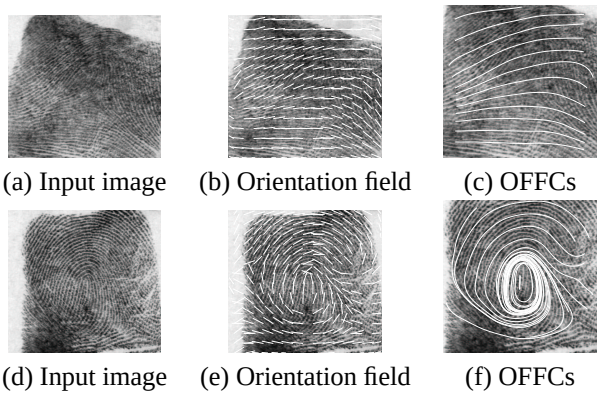

Figure 8. Noise in fingerprint images leading to errors in classification. The true and assigned classes of the fingerprints in the top (bottom) panels are left-loop and arch (left-loop and whorl), respectively.

one) sign-change points with local maximum and minimum values of +1 and -1, respectively, between locations of sign-change points. In Figures 4 (b), (d) and (f), we have plotted the graph of the isometric map for different left-loops of OFFCs in the corresponding right panels. The salient features of left-loop class remain the same: one sign-change point followed by one local minimum value of -1. Figures 5 (b), (d) and (f) give the isometric map plots of OFFC curves that are right-loops. Note that, similar to the left-loop, the features of the right-loop include one sign-change point followed by one local minimum value of -1. In the case of an arch type, the salient features include either (i) no sign-change points, or (ii) exactly one sign-point with the value of the local minimum far from -1. In order to determine whether a local maximum is close to or far way from +1, we use a threshold parameter, λ, $0 < \lambda < 1$. The value of a local maxima is determined to be close to +1 if it exceeds λ. Similarly, the value of a local minimum is determined to be close to -1 if its value falls below $-\lambda$.

Note that features of the isometric map plot cannot distinguish between a left- and a right-loop. Once an OFFC is determined to be of type loop, a further test is necessary to classify the OFFC as either a left- or a right-loop. In order to do this, we write each chord vector $V_j \equiv (V_j^x\,,\, V_j^y)^T$, and define $U_j = V_j^x \cdot V_j^y$. Left-loops correspond to sign changes of U_j from +1 to -1 and back to +1, whereas right-loops correspond to sign changes of U_j from -1 to +1 and back to -1.

3.4. Fingerprint Classification

Let N_T denote the total number of sampled OFFCs. We denote by $N_w\,,\, N_l\,,\, N_r\,,\, N_a$ to be the number of OFFCs labelled as whorl, left-loop, right-loop and arch ($N_w + N_l + N_r + N_a = N_T$). We select pre-specified threshold parameters λ_w, λ_l and λ_r to filter out noise in the labelling process. Our fingerprint classification procedure is described as follows: If $N_w \geq \lambda_w$, the fingerprint is assigned the class "whorl"; otherwise, we go to the next stage and consider the values of N_l, N_r and N_a. If $N_l \geq \lambda_l$ and $N_r < \lambda_r$, the fingerprint is classified as "left-loop"; if $N_l < \lambda_l$ and $N_r \geq \lambda_r$, the fingerprint is classified as right-loop. If both $N_l < \lambda_l$ and $N_r < \lambda_r$, the fingerprint class assigned is "arch".

4. Experimental Results

The methodology presented in the previous sections were validated on the NIST 4 fingerprint database [15]. The NIST 4 database contains 2,000 8-bit gray scale fingerprint image pairs, for a total of 4,000 images. Each image is 512-by-512 pixels with 32 rows of white space at the bottom and is classified into one of the following five classes: arch (A), left-loop (L), right-loop (R), tented arch (T) and whorl (W). The database is evenly distributed over the five classes with 800 fingerprints from each class. For our classification procedure, we combined classes "arch" and "tented arch" into a single "arch" class. The orientation field estimate was obtained using the approach described in [4].The estimate of the orientation field was obtained for the central part of the fingerprint image, leaving out a boundary of 50 pixels along each side of the image, that is, $r_{start} = c_{start} = 51$ and $r_{end} = c_{end} = 470$ (see Section 3.1). For obtaining each OFFC, we selected a step size of $l = 5$ pixels.

The threshold parameters for classification λ_w, λ_l and λ_r were fixed at $2, 2$ and 1, respectively. The value of λ was selected to be 0.90. The classification results are presented

Table 2. Classification results of fingerprints in the NIST4 database into four classes: A, L, R, and W

	Assigned Class					
True	A	L	R	W	Total	Accuracy (%)
A	797	2	1	0	800	99.62
T	781	19	0	0	800	97.62
L	63	730	1	6	800	91.25
R	75	4	720	1	800	90.00
W	12	23	18	747	800	93.34

in Table 2 with no reject option. For fingerprints that have two class labels, we determined that the assigned class is correct if it is one of the true labels. The overall accuracy of the classification procedure is obtained to be 94.4%. From Table 2, we see that the best classification was obtained for the class "arch" while the worst classification rates were obtained for the classes left-loop and right-loop. We note that our method of classification with no reject option achieves an accuracy that is comparable to the ones reported in the literature. Figure 7 shows the OFFCs for the five fingerprint classes in the Henry system shown in Figure 1. All these fingerprints have been correctly classified.

Sources of errors in our classification procedure can be assigned to one of the following factors. Spurious or missed patterns in the orientation field estimate, due to presence of random cuts and ink smudges in the fingerprint image, result in OFFCs with erroneous labels. Non-uniform illuminance at various regions of the fingerprint image severely distorts the ridge-valley structures and makes the extraction of a correct orientation field difficult (see Figure 8). Also, some left and right-loop fingerprints have a very small loop areas which are not detected by the extracted orientation field; these fingerprints are misclassified as arch.

5. Summary and Conclusions

An approach for identifying the geometric characteristics of OFFCs using graphs of tangent space isometric maps is developed. Salient features of the graphs are robust with respect to variations within each class of loops, whorls and arches, and are invariant under changes in translation, rotation and scaling. Left- and right-loops are distinguished using the sign changes that occur for the component-wise product of the tangent vectors. The class of a fingerprint is determined from the labels of each OFFC. Our classification procedure achieves a classification accuracy of 94.4%, a rate comparable to the ones reported in the literature. Future work will include detecting the smaller loop areas and classifying fingerprints into five Henry classes: left-loop, right-loop, whorl, arch and tented arch.

References

[1] R. Cappelli, A. Lumini, D. Maio, and D. Maltoni. Fingerprint classification by directional image partitioning. *IEEE Trans. on Pattern Analysis and Machine Intelligence*, 35:1209–1223, 2002.

[2] J. Chang and K. Fan. A new model for fingerprint classification by ridge distribution sequences. *Pattern Recognition*, 35:1209–1223, 2002.

[3] M. M. S. Chong, T. H. Ngee, L. Jun, and R. K. L. Gay. Geometric framework for fingerprint image classification. *Pattern Recognition*, 30(9):1475–1488, 1997.

[4] S. C. Dass. Markov random field models for directional field and singularity extraction in fingerprint images. *To appear in IEEE Trans. on Image Processing*, 2004.

[5] E. R. Henry. *Classification and Uses of Fingerprints*. London: Routledge, 1900.

[6] L. Hong and A. K. Jain. Classification of fingerprint images. *Proceedings of the 11th Scandinavian Conference on Image Analysis, Kangerlussuaq, Greenland*, June 7-11, 1999.

[7] A. K. Jain, S. Prabhakar, and L. Hong. A multichannel approach to fingerprint classification. *IEEE Transactions on Pattern Analysis and Machine Intelligence*, 21(4):348–359, 1999.

[8] K. Karu and A. K. Jain. Fingerprint classification. *Pattern Recognition*, 29(3):389–404, 1996.

[9] D. Maltoni, D. Maio, A. Jain, and S. Prabhakar. *Handbook of Fingerprint Recognition*. Springer-Verlag, New York, 2003.

[10] S. Minut and A. K. Jain. Hierarchical kernel fitting for fingerprint classification and alignment. *Proc. of International Conference on Pattern Recognition, Quebec City, August 11-15*, 2002.

[11] B. Moayer and K. S. Fu. A syntactic approach to fingerprint pattern recognition. *Pattern Recognition*, 7(1):1–23, 1975.

[12] B. Moayer and K. S. Fu. An application of stochastic languages to fingerprint pattern recognition. *Pattern Recognition*, 8:173–179, 1976.

[13] B. Moayer and K. S. Fu. A tree system appraoch for fingerprint pattern recognition. *IEEE Trans. Comput.*, 25(3):262–274, 1976.

[14] B. O'Neill. *Elementary Differential Geometry*. Academic Press, London, UK, 1997.

[15] C. I. Watson and C. L. Wilson. Nist special database 4, fingerprint database. *National Institute of Standards and Technology*, March 1992.

[16] C. L. Wilson, G. T. Candela, and C. I. Watson. Neural network fingerprint classifiaction. *J. Artificial Neural Networks*, 2:203–228, 1994.